Available online at www.sciencedirect.com
SCIENCE DIRECT®
Biochemical and Biophysical Research Communications 317 (2004) 930–938
BBRC
www.elsevier.com/locate/ybbrc

Homology modeling of the structure of tobacco acetohydroxy acid synthase and examination of the active site by site-directed mutagenesis☆

Dung Tien Le,[a] Moon-Young Yoon,[b] Young Tae Kim,[c] and Jung-Do Choi[a,*]

[a] *School of Life Sciences, Chungbuk National University, Cheongju 361-763, Republic of Korea*
[b] *Department of Chemistry, Hanyang University, Seoul 133-791, Republic of Korea*
[c] *Department of Microbiology, Pukyong National University, Busan 608-737, Republic of Korea*

Received 17 March 2004

Abstract

A reliable model of tobacco acetohydroxy acid synthase (AHAS) was obtained by homology modeling based on a yeast AHAS X-ray structure using the Swiss-Model server. Conserved residues at the dimer interface were identified, of which the functional roles of four residues, namely H142, E143, M489, and M542, were determined by site-directed mutagenesis. Eight mutants were successfully generated and purified, five of which (H142T, M489V, M542C, M542I, and M542V) were found to be inactive under various assay conditions. The H142K mutant was moderately altered in all kinetic parameters to a similar extent. In addition, the mutant was more thermo-labile than wild type enzyme. The E143A mutant increased the K_m value more than 20-fold while other parameters were not significantly changed. All mutations carried out on residue M542 inactivated the enzyme. Though showing a single band on SDS–PAGE, the M542C mutant lost its native tertiary structure and was aggregated. Except M542C, each of the other mutants showed a secondary structure similar to that of wild type enzyme. Although all the inactive mutants were able to bind FAD, the mutants M489V and M542C showed a very low affinity for FAD. None of the active mutants constructed was strongly resistant to three tested herbicides. Taken together, the results suggest that the residues of H142, E143, M489, and M542 are essential for catalytic activity. Furthermore, it seems that H142 residue is involved in stabilizing the dimer interaction, while E143 residue may be involved in binding with substrate pyruvate. The data from the site-directed mutagenesis imply that the constructed homology model of tobacco AHAS is realistic.

Keywords: Acetohydroxy acid synthase; Tobacco; Site-directed mutagenesis; Herbicide-resistance; Conserved residues; Multiple alignments; Homology modeling; Swiss-Model

Acetohydroxy acid synthase (AHAS, EC 4.1.3.18; also referred to as acetolactate synthase) catalyzes the first step in the biosynthesis of branched chain amino acids such as valine, leucine, and isoleucine in microorganisms and plants. AHAS catalyzes the condensation of two molecules of pyruvate to give rise to 2-acetolactate in the first step of the valine and leucine biosynthetic pathway, and in parallel, it also catalyzes the condensation of pyruvate and 2-ketobutyrate to yield 2-aceto-2-hydroxybutyrate in the second step of the isoleucine biosynthesis [1]. AHAS requires thiamine pyrophosphate (TPP), flavin adenine dinucleotide (FAD), and a divalent metal ion, Mg^{2+} or Mn^{2+} as cofactors for its catalytic function. Much attention has been paid to AHAS since it was demonstrated to be the target of several classes of herbicides, including the sulfonylureas [2,3], the imidazolinones [4], and the triazolopyrimidines [5,6].

AHAS activity is found in bacteria, yeast, and higher plants. Three bacterial AHAS isozymes have been purified and studied extensively with respect to their genetic regulation, kinetic properties, feedback regulation,

☆ *Abbreviations:* AHAS, acetohydroxy acid synthase; CD, circular dichroism; GSH, glutathione; GST, glutathione *S*-transferase; IPTG, isopropyl-β-D-thiogalactoside; PCR, polymerase chain reaction; TP, triazolopyrimidine sulfonamide; TPP, thiamine pyrophosphate.

* Corresponding author. Fax: +82-43-267-2306.
E-mail address: jdchoi@cbucc.chungbuk.ac.kr (J.-D. Choi).

0006-291X/$ - see front matter © 2004 Elsevier Inc. All rights reserved.
doi:10.1016/j.bbrc.2004.03.133

and sensitivity to herbicidal inhibitors [7–10]. Each of the isozymes is a tetramer of two large catalytic subunits (59–60 kDa) and two small regulatory subunits (9–17 kDa) [1]. In contrast to the bacterial enzyme, the structure and biochemical properties of AHAS from eukaryotes have not been well characterized since purification of eukaryotic AHAS is severely hampered by its extreme instability and very low abundance.

Recently, site-directed mutagenesis studies on tobacco AHAS in our laboratory revealed that K219 [11], W490 [12], C411 [13], H487 [14], and M512 [15] residues are essential for the catalytic function of tobacco AHAS, and that K255 [11], W573 [12], A121 [16], S652 [16], and M569 [15] are possibly located at the herbicide-binding site. More recently, crystallization and the preliminary X-ray diffraction analysis of the catalytic subunit of yeast AHAS were reported [17,18]. Until the X-ray structure of yeast AHAS was reported, several efforts had been made to understand the structural–functional relationship of AHAS by using homology modeling based on the X-ray structure of other TPP-dependent enzymes [19,20]. Ibdah et al. [19] reported the homology modeling and examination of the active site of bacterial AHAS, while Ott et al. [20] proposed an approach employing homology modeling and site-directed mutagenesis to design herbicide resistant AHAS.

Alignment of AHAS sequences from tobacco and yeast revealed a 41% and 63% sequence identity and similarity, respectively. Thus, in this study, we carried out homology modeling for catalytic subunits of tobacco AHAS based on the yeast AHAS X-ray structure (1JSC.pdb and 1N0H.pdb) using Deep View and the remote automatic modeling services at the Swiss-Model server. Multiple sequence alignment was also carried out for 39 AHAS sequences of plants and microorganisms. Conserved residues at the dimer interface were identified, among them the roles of four residues predicted to be at the active site (H142, E143, M489, and M542) were studied using site-directed mutagenesis. Residue Y494, a non-conserved residue and positioned away from the dimer interface, was also included in the study for comparison of the data.

Materials and methods

Materials. Bacto-tryptone, yeast extract, and Bacto-agar were purchased from Difco Laboratories (Detroit, USA). Restriction enzymes were purchased from Takara Shuzo (Shiga, Japan) and Boehringer–Mannheim (Mannheim, Germany). GSH, TPP, FAD, α-naphthol, and creatine were obtained from Sigma Chemical (St. Louis, USA). Thrombin protease and epoxy-activated Sepharose 6B were obtained from Pharmacia Biotech (Uppsala, Sweden). *Escherichia coli* XL1-Blue cells containing expression vector pGEX-ALS were provided by Dr. Soo-Ik Chang (Chungbuk National University, Cheongju, Korea). Oligonucleotides were obtained from Jenotech (Taejon, Korea). Londax (a sulfonylurea herbicide) and Cadre (an imidazolinone herbicide) were kindly provided by Dr. Dae-Whang Kim (Korea Research Institute of Chemical Technology, Taejon, Korea). TP, a triazolopyrimidine derivative, was obtained from Dr. Sung-Keon Namgoong (Seoul Women's University, Seoul, Korea).

Homology modeling of catalytic subunit of tobacco AHAS. AHAS sequences from tobacco and yeast were aligned using the program BioEdit [21]. Ninety-two N-terminal amino acid residues of the tobacco AHAS corresponding to the transit peptide were removed, the resultant sequences were fitted onto the X-ray structure yeast AHAS using the program Deep View. The resulting alignment was examined manually and then submitted for automatic modeling at the Swiss-Model server [22,23]. Two homodimer models of tobacco AHAS were obtained based on two different X-ray coordinates (with and without the presence of a herbicide, 1N0H.pdb, 1JSC.pdb). Structural illustrations were created by Deep View from the coordinate files [23].

Multiple sequence alignment of AHAS sequences. We aligned 39 AHAS sequences of plants and microorganisms using the program ClustalW [24], which was an integrated feature of the software BioEdit [21] provided by North Carolina State University. The data set consisted of AHAS sequences from the following species (GenBank accession numbers are given in parentheses): *A. powellii* (AAK50821), *A. retroflexus* (AAK50820), *A.* spp. (AAB67839), *A. thaliana* (P17597), *B. napus.* (P27818, P14874, and P27819), *B. scoparia* (AAC69629), *C. caldarium* (O19929), *Guillardia theta* (O78518), *N. tabacum* (CAA30484 and CAA30485), *P. purpurea* (P31594), *R. raphanistrum* (CAC86696), *S. platensis* (P27868), *S. ptychanthum* (AAG40281), *Volvox carteri* (AAC04854), *B. subtilis* (P37251 and Q04789), *A. pisum* (P57321), *S. graminum* (O85293), *S. chinensis* (Q9RQ65), *C. acetobutylicum* (AAC06204), *C. glutamicum* (P42463), *E. coli* (P08142, P00892, and P00893), *H. influenzae* (P45261), *K. pneumoniae* (P27696), *L. lactis* sub. *Lactis* (Q02137), *M. grisea* (AAB81248), *M. jannaschii* (Q57725), *M. avium* (Q59498), *M. leprae* (O33112), *M. tuberculosis* (O53250), *R. terrigena* (Q04524), *S. cerevisiae* (P07342), *S. typhimurium* (P40811), and *S. pombe* (P36620).

Site-directed mutagenesis. The site-directed mutagenesis of tobacco AHAS was performed directly on the plasmid derived from pGEX-2T containing tobacco AHAS cDNA, using the PCR megaprimer method [25]. All manipulations of the DNA were carried out using a previously recorded technique [26]. The PCR was also performed as described by Saiki et al. [27]. The first PCR was carried out with the oligonucleotide primer NKB2 and each mutagenic fragment was used as internal primer with the underlined base changed:

NKB2, 5′-CCCG**GGATCC**TCAAAGTCAATA-3′
H142K, 5′-CTACCACGTAAGGAGCAGG -3′
H142T, 5′-CTACCACGTACCGAGCAGG-3′
E143A, 5′-CCACGTCACGCTCAGGGT-3′
M489V, 5′-CAGGTTTGGGCAGCTCA-3′
Y494H, 5′-GGGCTGCTCAACACTATAACTAC-3′
M542C, 5′-GATGGCAGTTTTATCTGTAATGTG-3′
M542I, 5′-AGTTTCATCATCAATGTGCAG-3′
M542V, 5′-GTTTCATCGTTAATGTGCAGGAG-3′

The bold bases in the NKB2 primer are *Bam*HI restriction sites. The resulting DNA was subjected to a second PCR with the universal primer NKB1 5′-CATCTCC**GGATCC**ATGTCCACTACCCAA-3′. The PCR products were double digested with *Nco*I and *Bgl*II, and cloned into the expression vector, which was prepared from the *Nco*I/*Bgl*II-excised pGEX-wAHAS. The resulting pGEX-mAHAS was used to transform the *E. coli* strain XL1-Blue cells using standard $CaCl_2$ transformation instructions [30]. Each transformant was identified by the digestion of the plasmid with *Bam*HI, and followed by sequencing to ensure the correct base mutation. *E. coli* BL21(DE3) cells carrying the correct mutant AHAS plasmid were cultured to obtain the mutant protein.

DNA sequence analysis. DNA sequencing was carried out by the dideoxy chain-termination procedure [28] on an ABI Prism 3700 automatic DNA sequencer at Macrogen (Seoul, Korea). Each mutant AHAS was sequenced and identified.

Expression and purification of tobacco wAHAS and mAHAS. Bacterial strains of *E. coli* BL21(DE3) cells cells containing the expression vector pGEX-AHAS were grown at 37 °C in Luria–Bertani (LB) medium containing 50 μg/ml ampicillin to an OD_{600} of 0.7–0.8. Expression of the pGEX-AHAS gene was induced by adding 0.1–0.3 mM isopropyl-D-thiogalactoside (IPTG). Cells were grown for an additional 3 h at 30 °C and harvested by centrifugation at 5000*g* for 30 min. Purification of wAHAS and mAHAS was carried out by previously recorded techniques [12,15,16]. The cell pellets were suspended with the standard buffer (50 mM Tris–HCl, pH 7.5, 1 mM pyruvate, 10% (v/v) ethylene glycol, and 10 mM $MgCl_2$) containing protease inhibitors (2 μg/ml leupeptin, 4 μg/ml aprotinin, and 2 μg/ml pepstatin A). The cell suspension was then lysed by sonication at 4 °C. The homogenate was centrifuged at 20,000*g* for 20 min and the supernatant was recentrifuged. The supernatant was applied to the GSH-coupled Sepharose 6B column and unbound proteins were removed by washing with the standard buffer. Then, the GST-AHAS fusion protein was recovered from the column with an elution buffer (50 mM Tris–HCl, pH 7.5, 15 mM GSH, and 10% (v/v) ethylene glycol). To obtain the cleaved AHAS, the purified GST-AHAS was incubated overnight at 4 °C with thrombin (10 U/mg protein). The AHAS was purified by an additional step of GSH-affinity chromatography. The isolated protein was identified by SDS–PAGE analysis [29], and the protein concentration was determined by Bradford's method [30].

Enzymatic assay and determination of kinetic parameters. Enzyme activities of the purified wAHAS and mAHAS were measured according to Westerfeld's method [31] using a previously reported modification [32]. The reaction mixture contained a 50 mM potassium phosphate buffer (pH 7.5), 1 mM TPP, 10 mM $MgCl_2$, 20 μM FAD, 100 mM pyruvate, and the enzyme in the absence or presence of various concentrations of inhibitors. To determine thermo-stability of the enzyme, the enzyme was dissolved at the same concentration in an assay buffer (without substrate) and incubated at 60 °C. After a fixed period of time at 60 °C the tubes containing the enzyme were placed immediately on ice for 5 min before undergoing activity assay.

The values of V_{max} and K_m for the substrate were determined by fitting the data to Eq. (1), while the values of the activation constant (K_c) were obtained by fitting the data to Eq. (2). For error minimization, the non-linear least-squares and simplex methods were used [33]:

$$v = V_{max}/(1 + K_m/[S]), \quad (1)$$

$$v = V_0 + V_{max}/(1 + K_c/[C]). \quad (2)$$

In these equations, v is the reaction velocity, V_{max} is the maximum velocity, V_0 is the residual activity due to the trace of cofactors present in enzyme solution, K_m is the Michaelis–Menten constant, K_c is the activation constant, [S] is the substrate concentration, and [C] is the added cofactor concentration. The K_i^{app} was determined by fitting the data to Eq. (3)

$$v_i = v_0/(1 + [I]/K_i^{app}). \quad (3)$$

In this equation, v_i and v_0 represent the reaction velocities in the presence or absence of the inhibitor, respectively, and [I] is the concentration of the inhibitor. The K_i^{app} is the apparent K_i, that is the concentration of the inhibitor giving 50% inhibition under a standard assay condition, which is also known as IC_{50}.

Spectroscopic measurement. Absorption spectra were recorded on a Beckman DU-600 spectrophotometer. The protein solution was dispensed in 1 ml black-walled quartz cuvettes, and the spectrum of each sample was scanned over the range of 250–550 nm. The fluorescence spectra of FAD bound to wAHAS and mAHAS were scanned over the range of 450–650 nm by exciting at 450 nm on a Perkin–Elmer Luminescence spectrophotometer LS50B. The far-UV CD spectra were recorded over the range of 190–250 nm on a Jasco J-710 Spectropolarimeter set at 20–50 mdeg sensitivity, 1 mm resolution, 3 U accumulation, 5 s response, and at a scanning speed of 200 nm/min. A protein solution of 0.15–0.3 mg/ml was assayed in a 1 mm-path length cylindrical quartz cell. Near-UV CD spectra were measured using a 20 mm-path length cylindrical quartz cell.

Results

Homology models of tobacco AHAS

The pair-wise alignment of tobacco and yeast AHAS sequences revealed a 41% sequence identity and a 63% sequence homology (data not shown). Using the approach as described in Materials and methods two models based on two separate X-ray coordinates of yeast AHAS were obtained. The RMS *Z*-scores returned by WhatCheck [34,35] (data not shown) showed that the models obtained were acceptable and the Ramachandran plot [36] (Fig. 1) showed that the overall conformation of the backbone of the model was reliable.

On the model, we have identified more than a hundred residues on each subunit located at the dimer interface. After considering the multiple sequence alignment data (data not shown), the following residues were selected for site-directed mutagenesis study; H142, E143, M489, Y494, and M542.

His142 mutants

On the model generated, H142 was found to interact with Q144 of the other subunit (Fig. 8). In addition, it was identical among 39 AHAS sequences (data not shown). To understand the roles of the residue H142,

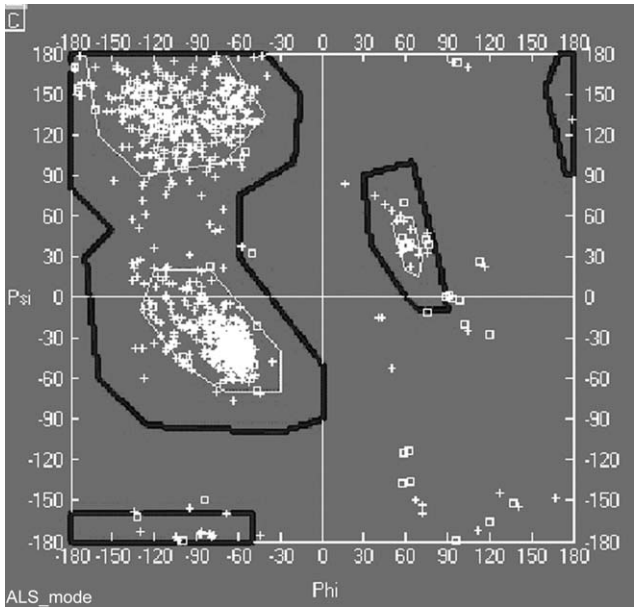

Fig. 1. Ramachandran plot of the main-chain dihedral angles (Φ, Ψ) for tobacco AHAS dimer model. The rectangular sign represents glycine residues, the plus sign represents other residues.

two substitutions, H142T and H142K, were carried out. The two mutants expressed as intact proteins (data not shown), however, the H142T mutant did not give any measurable activity under various assay conditions, while the H142K mutant showed an activity level equivalent to 17% of that given by wild type enzyme (Table 1). However, its K_m value was 18-fold higher than that of the wild type. The protein concentration dependence of specific activity showed that, a linear pattern was observed with wild type enzyme, while with the H142K mutant, a non-linear behavior was observed (Fig. 2). Furthermore, the H142K mutant was less stable at 60 °C than wild type enzyme. As shown in Fig. 3, the half-time of H142K mutant was 43.5 s while for wild type enzyme this value was 62.8 s. The H142K mutant was moderately resistant to three tested herbicides, Londax, Cadre, and TP (Table 1 and Fig. 7). The fluorescence emission spectra of the two mutants showed a peak corresponding to the present of FAD (Fig. 4 inset and data not shown). The secondary structures of the two mutants, as detected by CD spectra, were similar to that of wild type enzyme (Fig. 5A). The size-exclusion chromatograph showed that the H142T mutant was able to form an oligomer complex similar to the active complex of the wild type enzyme (data not shown).

Glu143 mutant

The residue of yeast and *E. coli* AHAS equivalent to E143 in the tobacco AHAS was identified to involve in catalysis [1,37]. In our model, the residue E143 was found to contribute one hydrogen bond to TPP molecule (Fig. 8). The residue is also identical in the 39 AHAS sequences examined. To determine the function of the residue E143, the mutant carrying E143A was constructed. The mutation yielded an enzyme with 43% specific activity in comparison with that of wild type enzyme, however, its K_m value was 23-fold higher than that of wild type enzyme (Table 1). The mutant was able to bind FAD, as detected by the fluorescence emission spectrum (data not shown),

Table 1
Kinetic parameters of wild type and mutant enzymes

	K_m (mM)	V_{max} (U/mg protein)	K_{FAD} (μM)	K_{TPP} (mM)	K_i^{app}		
					Cardre (μM)	Londax (nM)	TP (μM)
wALS	5.45	1.74	4.56	0.29	6.59	8.80	18.87
H142K	94.9	0.30	2.61	0.21	123.22	195.46	34.87
H142T	No enzymatic activity						
E143A	126.47	0.75	7.06	0.16	2.67	8.32	12.69
M489V	No enzymatic activity						
Y494H	4.04	1.21	0.59	0.14	5.06	7.44	28.49
M542C	No enzymatic activity						
M542I	No enzymatic activity						
M542V	No enzymatic activity						

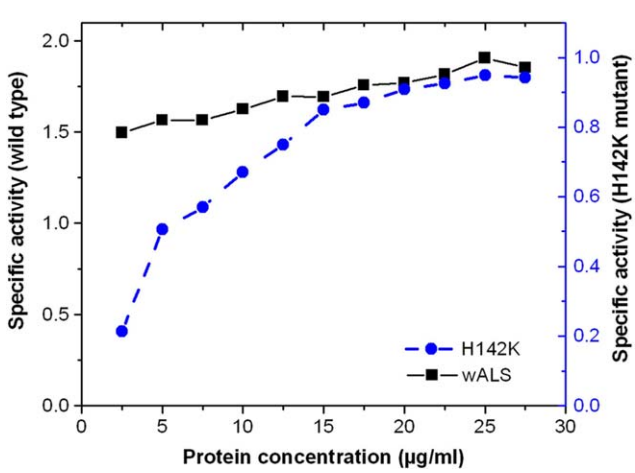

Fig. 2. Protein concentration dependence of the specific activity of wild type and H142K mutant enzymes. The activity of wild type and mutant enzymes was measured as described in Materials and methods in saturated concentrations of cofactors. Reaction times for the wild type and the mutant were 8 and 40 min, respectively.

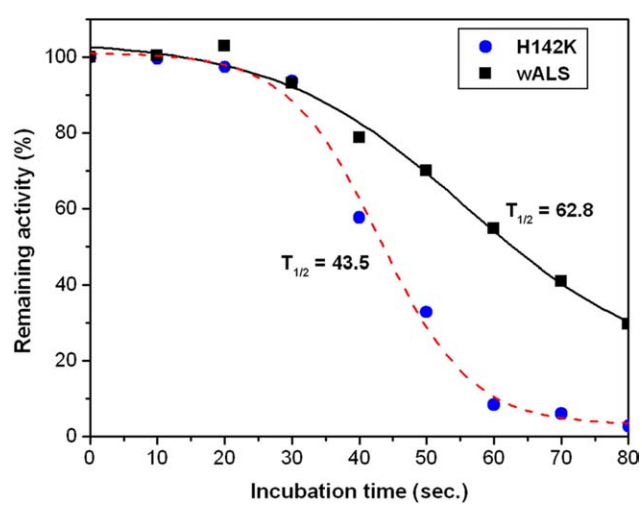

Fig. 3. Thermo-stability of the H142K mutant and wild type enzyme. Each enzyme was present at the same concentration in assay buffer; the enzyme was incubated at 60 °C for different periods of time, cooled down on ice immediately, and then used for activity assay.

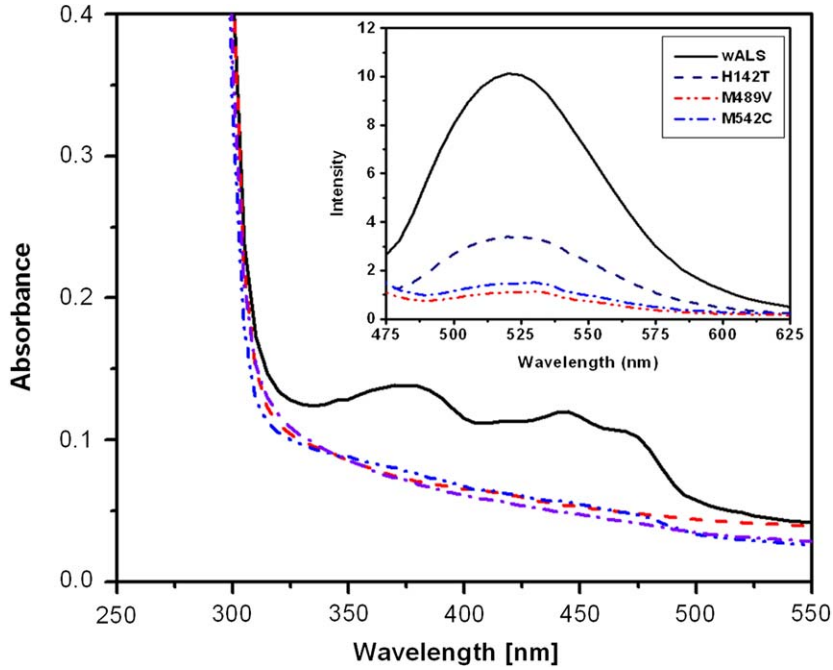

Fig. 4. Absorption and fluorescence spectra of wild type and mutant enzymes. The concentration of each enzyme was 0.9 mg protein/ml in 50 mM Tris–Cl buffer (pH 7.5).

and its far-UV CD spectrum was similar to that of wild type enzyme (Fig. 5C). The sensitivity of the E143A mutant to the three tested herbicides, Londax, Cadre, and TP, was also similar to that of wild type enzyme (Fig. 7).

Met489 mutant

This residue was located 9 Å from the dimer interface, and 4 Å from the nearest part of the FAD molecule, it is also conserved in 36 out of 39 AHAS sequences. The M489V mutant was found to be inactive under various assay conditions, although it was expressed as intact protein similar to that of wild type enzyme, as judged by SDS–PAGE (data not shown). The binding of FAD was hardly detected with this mutant by either absorbance or fluorescence emission spectra (Fig. 4). Its secondary structure, determined by CD spectrum, resembled that of wild type enzyme (Fig. 5B).

Met542 mutants

Our homology model shows that the residue M542 is located within 6 Å from the dimer interface, and came within close proximity to the TPP molecule (within 3.5 Å, Fig. 8). Though it does not directly interact with the TPP molecule, it is hydrogen-bonded to the residue S539, which is bonded to TPP along with the residues G536, D537, and G538. These residues belong to the TPP-binding motifs ($GDGX_{24–27}NN$) [38]. Three substitutions were carried out on this residue and yielded M542C, M542I, and M542V mutants. The three mutants were purified and showed a single band on SDS–PAGE similar to wild type enzyme (data not shown). However, all the mutants were inactive under various assay conditions. The far-UV CD spectrum of the M542C mutant was substantially different from that of wild type enzyme, while the spectra of the other two mutants, M542I and M542V, overlapped with that of wild type enzyme (Fig. 5C and data not shown). The near-UV CD spectrum of the M542C mutant showed that it had lost the tertiary structure (Fig. 6). The size-exclusion chromatograph showed that the M542C mutant was aggregated, as it did not have an elution peak corresponding to the active complex of wild type enzyme (data not shown).

Tyr494 mutant

This residue is located far away from the dimer interface (>20 Å), in addition it is also not well conserved in the 39 AHAS sequences. The mutant carrying Y494H substitution was constructed. Its kinetic parameters, including V_{max}, K_m, K_c for cofactors and K_i^{app} for the three tested herbicides, were similar to that of wild type enzyme (Table 1 and Fig. 7). The level of FAD in the enzyme solution, determined by absorbance and fluorescence emission spectra, was comparable with that of wild type enzyme (data not shown). No change in its secondary structure was observed when its CD spectrum was compared with that of wild type enzyme (data not shown).

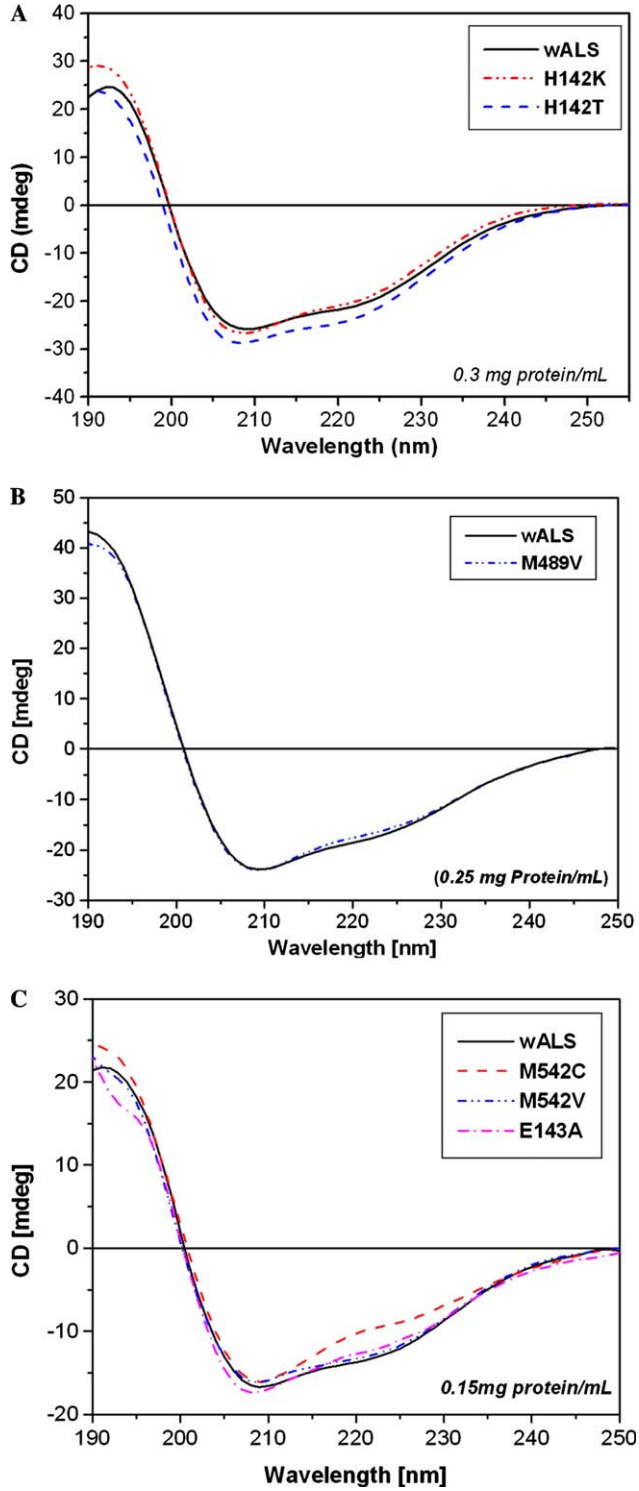

Fig. 5. Far-UV CD spectra of wild type and mutant enzymes. Each protein was present at a concentration ranging from 0.15 to 0.30 mg/mL in 10 mM potassium phosphate buffer (pH 7.5). Spectra were recorded using 1 mm-path length cylindrical quartz cell.

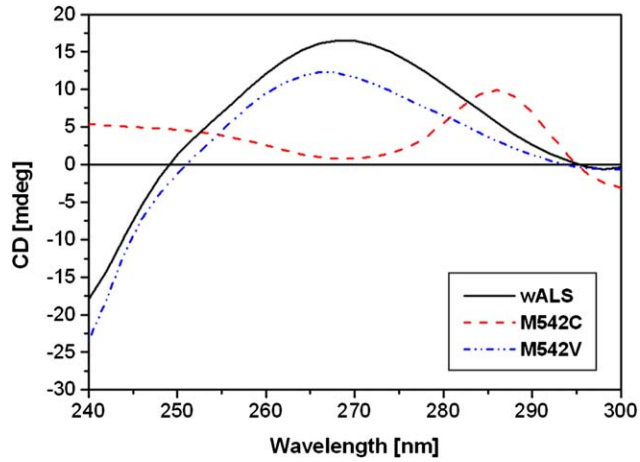

Fig. 6. Near-UV CD spectra of wild type and mutant enzymes. Each protein was present at a concentration of 0.20 mg/mL in 10 mM potassium phosphate buffer (pH 7.5). Spectra were recorded using 20 mm-path length cylindrical quartz cell.

Discussion

So far, there has been no report on the X-ray structure of plant acetohydroxy acid synthase. Thus, a complete 3D structural model of tobacco AHAS will be useful to understand the structure–function relationship of plant AHAS. Previously, several efforts had been made to understand the structure and catalysis mechanism of AHAS by employing homology modeling [19,20]. However, their homology models were based exclusively on pyruvate oxidase, a TPP-dependent enzyme. Ibdah et al. [19] employed homology modeling to study the active site of bacterial AHAS, while Ott et al. [20] used this approach to design herbicide resistant AHASs.

Recently, Pang et al. [17,18] reported the crystallization and the X-ray diffraction study on yeast AHAS. The sequence homology between yeast and tobacco AHASs was higher than that between tobacco AHAS and pyruvate oxidase sequences. Though the resolution of the yeast AHAS X-ray structure was relatively low (2.6 and 2.8 Å), it is a good template to carry out homology modeling for the structure of tobacco AHAS. To carry out the homology modeling of tobacco AHAS based on the X-ray structure of yeast AHAS, we exclusively relied on Swiss-Model, which uses Deep View to perform optimization. The automatic modeling was done at the Swiss-Model server located in Switzerland [22,23].

Pang et al. [18] reported two different X-ray coordinates. The one resolved at 2.6 Å resolution (PDB Accession No. 1JSC) was without a herbicide while the other resolved at 2.8 Å resolution (PDB Accession No. 1N0H) was with a herbicide [18]. We have generated two models based on these two coordinates. The calculated pair-wise RMSD of the model and its template (1JSC.pdb) was 0.86 Å. Since it had been proposed that the dimerization of the catalytic subunits seems to be required for activity [39] we were thus interested in examining the dimer interface residues. Based on the models generated, we identified more than a hundred

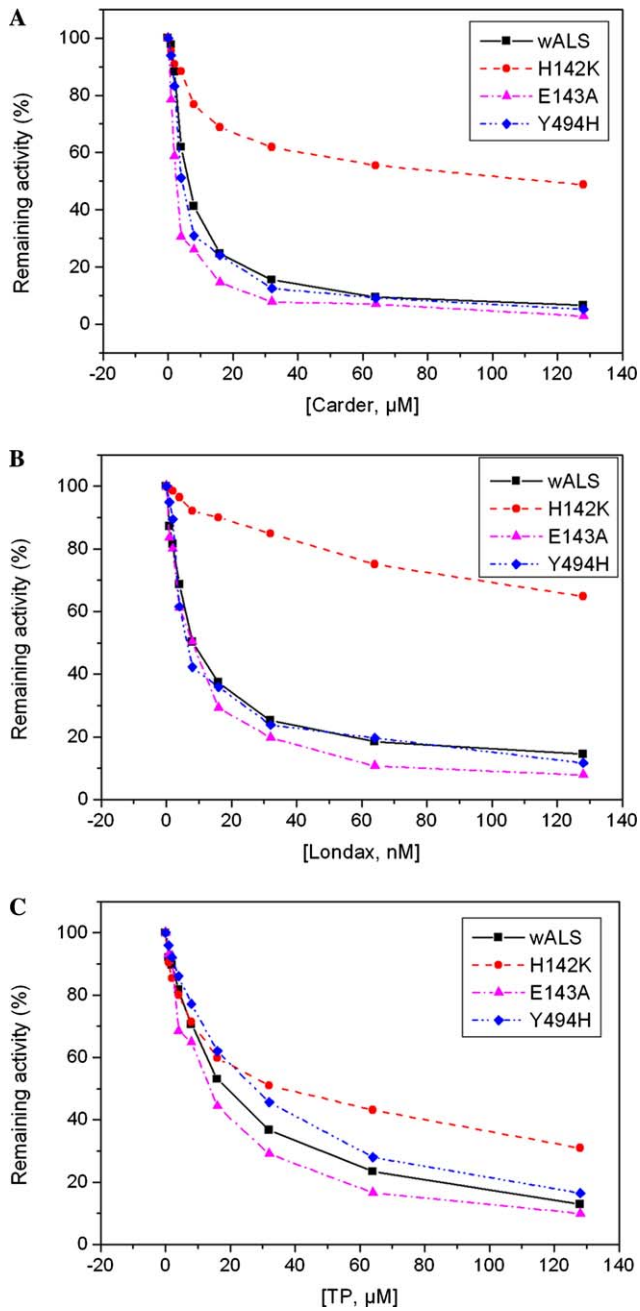

Fig. 7. Effects of three tested herbicides (the sulfonylurea Londax, the imidazolinone Cardre, and the triazolopyrimidine TP) on wild type and mutant enzymes.

residues located 6 Å within the dimer interface. Among these residues, we selected only the well-conserved residues by carrying out a multiple sequence alignment for 39 AHAS sequences.

The loop containing H142, E143, and Q144 was of interest because an equivalent residue to E143 in yeast was found to have hydrogen-bonded to the TPP molecule. In addition, its equivalent residues of AHAS from other species were identified to be involved in catalysis [1,37]. From the model, the side chain of residue H142 was found to make an H-bond to the side chain of Q144, which is also well conserved, of the other subunit (Fig. 8). Thus, we supposed that these residues play important roles in the normal function of the enzyme.

To understand the roles of H142 and its interaction with Q144 in the normal function of the enzyme, we replaced H142 by either threonine or lysine and yielded two mutants carrying H142T and H142K substitutions, respectively. On the model, these two mutations broke the H-bond between H142 and Q144. Experimentally, we found that the H142T mutant was inactive under various assay conditions, while the H142K mutant remained active but its kinetic parameters, including V_{max}, K_m, and K_i^{app} for the three classes of herbicides, were moderately altered to a similar extent (Table 1 and Fig. 7). Bar-Ilan et al. reported that the isozyme AHAS II from *E. coli* is tightly associated as its protein concentration dependence of specific activity was linear and constant [37]. However, in tobacco AHAS, we show here that, the behavior is linear ($R = 0.981$) but not constant within the range of 2.5–37.5 μg/ml of protein concentration. In fact, the specific activity of the enzyme slightly increases when protein concentration increases with a slope of 0.0155 (Fig. 2). In contrast, the protein concentration dependence of the specific activity of the H142K mutant was non-linear. Data on Fig. 2 show that, the behavior of the H142K mutant was similar to that of the wild type only if its protein concentration was greater than 15 μg/ml. This behavior can be explained by an increased dissociation of the subunits of the mutant in comparison to the wild type at concentrations of protein less than 15 μg/ml.

Furthermore, the H142K mutant was more thermolabile than wild type enzyme (Fig. 3). The spectral data of these two mutants showed that they can bind FAD and the mutation did not cause any change in the secondary structure of the enzyme (Figs. 4 and 5 and data not shown). Though the interaction between H142 and Q144 was disrupted in the H142T mutant, the size-exclusion study showed that the enzyme, despite being inactive, can still form the oligomer complex like that of wild type enzyme when they are at the same protein concentration of 1.0 mg/ml (data not shown). In a protein molecule, histidine behaves like a charge residue, hence, the substitution by lysine, a charge residue, can be considered as a "conservative substitution." The overall data suggest that H142 is essentially located at the active site, and that the side chain of H142 may be crucial for catalytic activity. The interaction between H142 and Q144 of the other subunit is important in the association of the subunits to form the dimer complex, and hence, it is crucial for the correct conformation of the active site.

To determine the function of residue E143, a mutant carrying E143A substitution was generated. The experimental data showed that, the mutation of E143 by alanine did not inactivate the enzyme. In fact, the E143A

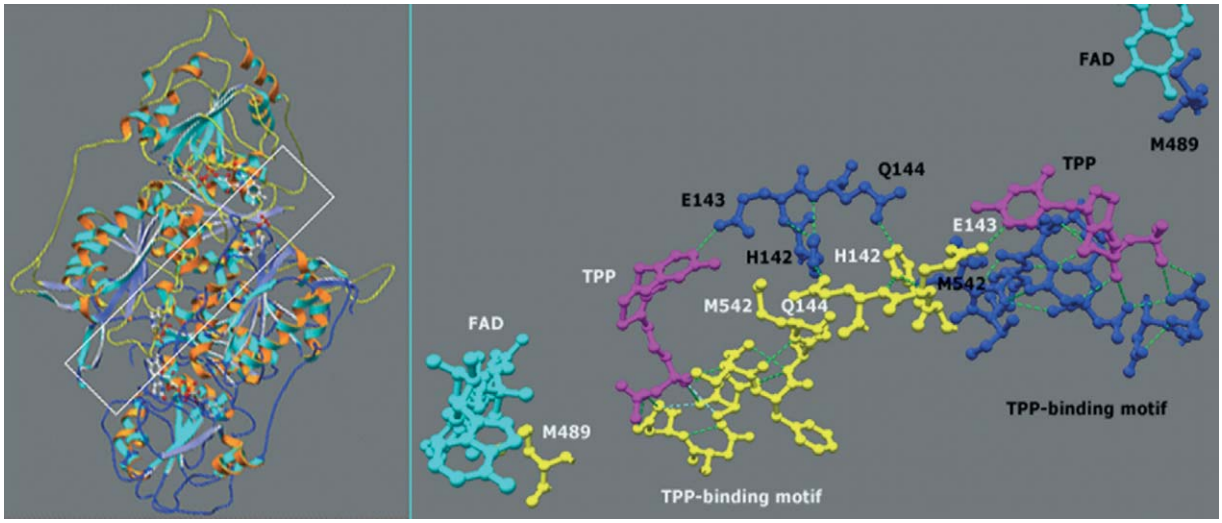

Fig. 8. Structure at the active site of the enzyme. Figure was generated by Deep View using the coordinate file of the model. Left, dimer model. Right, magnified dimer interface showing two active sites corresponding to two subunits. Residues in yellow belong to subunit A, those in deep blue belong to subunit B. TPP molecules are in violet.

mutant only increased the K_m value 23-fold for pyruvate, while other parameters, including V_{max} and K_i^{app} for the three tested herbicides, remained negligibly affected. These data suggested that E143 is located at the active site and probably involved in binding with pyruvate. Our data are also in agreement with those reported by Bar-Ilan et al. on AHAS II from *E. coli*. In their study, the mutant carrying an equivalent mutation (E47A) was active, but its K_{cat}/K_m value was severely reduced [37].

Previously, we reported the functional roles of three well conserved methionine residues (M350, M512, and M569) in tobacco AHAS [15]. On the model, the residue M489 located 9 Å from the dimer interface and just 4 Å from the FAD molecule. The residues M542 located 6 Å from the dimer interface and close in proximity to the TPP molecule. Indeed, the residue M542 interacts with a residue (S539) within the TPP binding motif. In addition, these two residues are well conserved in the 39 AHAS sequences.

In the experimental part, we found that the mutation of M489V inactivated the enzyme (Table 1). Moreover, the mutation abolished the binding affinity of the enzyme for FAD cofactor (Fig. 4), while its secondary structure was not changed (Fig. 5). It is likely that M489 is involved in binding with FAD, which is required for the correct formation of the enzyme.

To understand the functions of residue M542, we carried out three replacements. All mutants (M542C, M542I, and M542V) turned out to be practically inactive. The spectral (Figs. 4–6) and size-exclusion chromatography (data not shown) data showed that the M542C mutant hardly bound the FAD cofactor and also lost its tertiary structure. On the other hand, the two mutants, M542I and M542V, were able to bind the FAD cofactor (Fig. 4 and data not shown), and their secondary structures were similar to that of wild type enzyme (Figs. 5 and 6 and data not shown). The data obtained here supported that the residue M542 is located at the active site of the enzyme, and that substitutions at this residue may disturb the TPP-binding motif.

The residue Y494 was less conserved and located far away from the dimer interface (20 Å). It was included in this study for the purpose of data comparison. It is not surprising that the Y494H mutant showed similar properties as those of wild type enzyme.

Taking into account the data presented in this paper, it is likely that the residues H142, E143, M489, and M542 are located at the active site of the enzyme. Furthermore, residue H142 is possibly involved in the interaction with the other subunits, residue E143 may be involved in binding with substrate pyruvate and hence determines the substrate specificity of the enzyme, residue M489 seems to be responsible for binding with the FAD cofactor, and residue M542 is vital for the catalytic activity. The experimental data illustrate that the homology model is realistic.

Acknowledgments

We thank Dr. Dae-Whang Kim (Korea Research Institute of Chemical Technology, Korea) for providing us with Londax and Cadre, and Dr. Sung-Keon Namgoong (Seoul Women's University, Korea) for providing us with TP. This work was supported by Korea Research Foundation Grant KRF-2002-070-C0064.

References

[1] R.G. Duggleby, S.S. Pang, Acetohydroxyacid synthase, J. Biochem. Mol. Biol. 33 (2000) 1–36.

[2] R.A. LaRossa, J.V. Schloss, The sulfonylurea herbicide Sulfometuron is an extremely potent and selective inhibitor of acetolactate synthase in *Salmonella typhimurium*, J. Biol. Chem. 259 (1984) 8753–8757.
[3] J.B. Ray, Site of action of chlorosulfuron: inhibition of valine and isoleucine biosynthesis of plants, Plant Physiol. 75 (1984) 827–831.
[4] D.L. Shaner, P.C. Anderson, M.A. Stidham, Imidazolinones: potent inhibitors of acetohydroxy acid synthase, Plant Physiol. 76 (1984) 545–546.
[5] B.C. Gerwick, M.V. Subramanian, V. Loney-Gallant, D.P. Chander, Mechanism of action of the 1,2,4-triazolo[1,5,a-]pyrimidine, Pestic. Sci. 29 (1990) 357–364.
[6] S.K. Namgoong, H.J. Lee, Y.S. Kim, J.-H. Shin, J.-K. Che, D.Y. Jang, G.S. Kim, J.W. Yoo, M.-K. Kang, M.-W. Kil, J.-D. Choi, S.-I. Chang, Synthesis of the quinoline-linked triazolopyrimidine analogues and their interactions with the recombinant tobacco acetolactate synthase, Biochem. Biophys. Res. Commun. 258 (1999) 797–801.
[7] J.V. Schloss, K.E.V. Dyk, J.F. Vasta, B.M. Kutny, Purification and properties of *Salmonella typhimurium* acetolactate synthase isozyme II from *Escherichia coli* HB101/pDU9, Biochemistry 24 (1985) 4952–4959.
[8] Z. Barak, D.M. Chipman, N. Gollop, Physiological implications of the specificity of acetohydroxy acid synthase isozymes, J. Bacteriol. 169 (1989) 3750–3756.
[9] L. Eoyang, P.M. Silverman, Purification and assays of acetolactate synthase I from *Escherichia coli* K12, Methods Enzymol. 166 (1988) 435–445.
[10] C.M. Hill, R.G. Duggleby, Mutagenesis of *Escherichia coli* acetohydroxy acid synthase II and characterization of three herbicide-resistant forms, Biochem. J. 335 (1998) 653–661.
[11] T.-Y. Yoon, S.-M. Chung, S.-I. Chang, M.-Y. Yoon, T.-R. Hahn, J.-D. Choi, Roles of lysine 219 and 255 residues in tobacco acetolactate synthase, Biochem. Biophys. Res. Commun. 293 (2002) 433–439.
[12] C.-K. Chong, H.-J. Shin, S.-I. Chang, J.-D. Choi, Role of tryptophanyl residues in tobacco acetolactate synthase, Biochem. Biophys. Res. Commun. 259 (1999) 136–140.
[13] H.-J. Shin, C.-K. Chong, S.-I. Chang, J.-D. Choi, Structural and functional role of cysteinyl residues in tobacco acetolactate synthase, Biochem. Biophys. Res. Commun. 271 (2000) 801–806.
[14] K.-J. Oh, E.-J. Park, M.-Y. Yoon, J.-R. Han, J.-D. Choi, Roles of histidine residues in tobacco acetolactate synthase, Biochem. Biophys. Res. Commun. 282 (2001) 1237–1243.
[15] D.T. Le, M.-Y. Yoon, Y.T. Kim, J.-D. Choi, Roles of conserved methionine residues in tobacco acetolactate synthase, Biochem. Biophys. Res. Commun. 306 (4) (2003) 1075–1082.
[16] C.-K. Chong, J.-D. Choi, Amino acid residues conferring herbicide tolerance in tobacco acetolactate synthase, Biochem. Biophys. Res. Commun. 279 (2000) 462–467.
[17] S.S. Pang, L.W. Guddat, R.G. Duggleby, Crystallization of the catalytic subunit of *Saccharomyces cerevisiae* acetohydroxyacid synthase, Acta Crystallogr. D 57 (2001) 1321–1323.
[18] S.S. Pang, L.W. Guddat, R.G. Duggleby, Molecular basis of sulfonylureas herbicide inhibition of acetohydroxyacid synthase, J. Biol. Chem. 278 (2003) 7639–7644.
[19] M. Ibdah, A. Bar-Ilan, O. Livnah, J.V. Schloss, Z. Barak, D.M. Chipman, Homology modeling of the structure of bacterial acetohydroxy acid synthase and examination of the active site by site-directed mutagenesis, Biochemistry 35 (1996) 16282–16291.
[20] K.-H. Ott, J.-G. Kwagh, G.W. Stockton, V. Sidrov, G. Kekefuva, Rational molecular design and genetic engineering of herbicide resistance crops by structure modeling and site-directed mutagenesis of acetohydroxyacid synthase, J. Mol. Biol. 263 (1996) 359–367.
[21] T.A. Hall, BioEdit: a user-friendly biological sequence alignment editor and analysis program for Windows 95/98/NT, Nucleic Acids Symp. Ser. 41 (1999) 95–98.
[22] T. Schwede, J. Kopp, N. Guex, M.C. Peitsch, Swiss-Model: an automated protein homology-modeling server, Nucleic Acids Res. 31 (2003) 3381–3385.
[23] N. Guex, M.C. Peitsch, Swiss-Model and the Swiss-PdbViewer: an environment for comparative protein modelling, Electrophoresis 18 (1997) 2714–2723.
[24] J.D. Thompson, D.G. Higgins, T.J. Gibson, CLUSTALW: improving the sensitivity of progressive multiple sequence alignment through sequence weighting, positions-specific gap penalties and weight matrix choice, Nucleic Acids Res. 22 (1994) 4673–4680.
[25] G. Sarkar, S.S. Sommer, "Megaprimer" method of site-directed mutagenesis, Biotechniques 2 (1990) 404–407.
[26] J. Sambrook, E.F. Fritsch, T. Maniatis, Molecular Cloning: A Laboratory Manual, second ed., Cold Spring Harbor Laboratory Press, Cold Spring Harbor, New York, USA, 1989.
[27] R.K. Saiki, D.H. Gelfand, S. Stoffel, S.J. Scharf, R. Higuchi, G.T. Horn, K.B. Mullis, H.A. Erlich, Primer-directed enzymatic amplification of DNA with a thermostable DNA polymerase, Science 239 (1988) 487–491.
[28] F. Sanger, S. Nicklen, A.R. Coulson, DNA sequencing with chain-terminating inhibitors, Proc. Natl. Acad. Sci. USA 74 (1977) 5463–5467.
[29] U.K. Laemmli, Cleavage of structural proteins during the assembly of the head of bacteriophage T4, Nature 227 (1970) 680–685.
[30] M.M. Bradford, A rapid and sensitive method for the quantification of microgram quantities of protein utilizing the principle of protein-dye binding, Anal. Biochem. 72 (1976) 248–254.
[31] W.W. Westerfeld, A colorimetric determination of blood acetoin, J. Biol. Chem. 161 (1945) 495–502.
[32] C.-K. Chong, S.-I. Chang, J.-D. Choi, Functional amino acid residues of recombinant tobacco acetolactate synthase, J. Biochem. Mol. Biol. 30 (1997) 274–279.
[33] J.A. Nelder, R. Mead, A simplex method for function minimization, Comput. J. 7 (1965) 308–313.
[34] R.W.W. Hooft, G. Vriend, C. Sander, E.E. Abola, Errors in protein structures, Nature 381 (1996) 272.
[35] G. Vriend, WHAT IF: a molecular modeling and drug design program, J. Mol. Graph. 8 (1990) 52–56.
[36] G.N. Ramachandran, C. Ramakrishnan, V. Sasisekharan, Stereochemistry of polypeptide chain conformations, J. Mol. Biol. 7 (1963) 95–99.
[37] A. Bar-Ilan, V. Balan, K. Tittmann, R. Golbik, M. Vyazmensky, G. Hubner, Z. Barak, D.M. Chipman, Binding and activation of thiamin diphosphate in acetohydroxyacid synthase, Biochemistry 40 (2001) 11946–11954.
[38] C.F. Hawkins, A. Borges, R.N. Perham, A common structural motif in thiamin pyrophosphate-binding enzymes, FEBS Lett. 255 (1989) 77–82.
[39] M. Vyazmensky, C. Sella, Z. Barak, D.M. Chipman, Isolation and characterization of subunits of acetohydroxy acid synthase isozyme III and reconstitution of the holoenzyme, Biochemistry 35 (1996) 10339–10346.